Miniature probe combining optical-resolution photoacoustic microscopy and optical coherence tomography for *in vivo* microcirculation study

Lei Xi,[1] Can Duan,[2] Huikai Xie,[2] and Huabei Jiang[1,*]

[1]Department of Biomedical Engineering, University of Florida, Gainesville, Florida 32611, USA

[2]Department of Electrical and Computer Engineering, University of Florida, Gainesville, Florida 32611, USA

*Corresponding author: hjiang@bme.ufl.edu

Received 9 January 2013; revised 17 February 2013; accepted 21 February 2013;
posted 22 February 2013 (Doc. ID 181482); published 14 March 2013

Photoacoustic microscopy (PAM) is sensitive to optical absorption, while optical coherence tomography (OCT) is based on optical backscattering. Combining PAM and OCT can provide complementary information about biological tissue. Here we present a combined optical-resolution PAM (ORPAM) and OCT system that is integrated through a miniature probe with an overall diameter of 2.3 mm, suitable for insertion through a standard endoscopic or laparoscopic port during minimally invasive surgery or endoscopic exam. The hybrid probe consists of a common optical path for OCT (light delivery/detection) and ORPAM (light excitation) and a 10 MHz unfocused ultrasound transducer for photoacoustic detection. The combined system yields a lateral resolution of 15 μm for both ORPAM and OCT. © 2013 Optical Society of America

OCIS codes: 110.0110, 130.0130, 180.0180.

1. Introduction

Photoacoustic microscopy (PAM), especially optical-resolution PAM (ORPAM), is an emerging tool for three-dimensional (3D) visualizing biological tissue *in vivo* with high resolution [1–5]. Different from conventional microscopy techniques, ORPAM is fundamentally sensitive to optical absorbers in tissue such as hemoglobin and melanin, making it ideal for imaging blood vessels [2]. However, it is currently impossible for ORPAM to image scatterers in tissue. Several recent studies have attempted to combine photoacoustic imaging with other modalities, such as diffuse optical tomography (DOT) [6–8] and optical coherence tomography (OCT) [9,10], so that both the absorption and the scattering features of tissue can be imaged with the combined imaging modalities. The major drawback of these integrated systems, however, is that the systems are bulky and thus cannot be employed in endoscopic or intravascular visualization.

In this regard, several groups have made efforts to combine photoacoustic imaging with ultrasound or OCT for endoscopic or intravascular imaging. An integrated photoacoustic and ultrasound endoscopic probe with an outer diameter of 3.5 mm was reported in [11]. In this probe, a focused ultrasound transducer with a hole in the center for optical illumination was used coupled with a micromotor for internal scanning. The combination of photoacoustic imaging and ultrasound was also demonstrated for intravascular imaging [12]. In another study, Yang et al. reported an endoscopic probe with a size of 5 mm in diameter for ovarian cancer detection where three separated miniature probes for photoacoustic tomography, OCT and ultrasound, respectively, were bundled [13]. Due to the different light paths used for OCT and photoacoustic illuminations, it was

1559-128X/13/091928-04$15.00/0

difficult to coregister the photoacoustic and OCT images.

In this work, we present for the first time, to the best of our knowledge, the combination of ORPAM and OCT based on a miniature probe only 2.3 mm in diameter, which will be ideal for endoscopic and intravascular imaging. The optical paths of both ORPAM and OCT are built upon a single-mode fiber, a miniature gradient index (GRIN) lens, and two microprisms, enabling these two modalities to scan the same tissue area. The self-focusing ability of the GRIN lens results in a highly focused light beam for OCT and ORPAM, yielding a high lateral resolution of 15 μm for both modalities.

2. Materials and Methods

Figure 1(a) shows the schematic of the integrated probe. In this probe, the illumination beams for both OCT and ORPAM are coupled into one tip of a single-mode fiber (SMF-28e^+, Thorlabs) with 0.14 NA and 0.9 mm outer diameter. The other tip of the fiber is cut with an 8° angle to minimize backreflection. Optical UV glue is used to connect the fiber tip with the GRIN lens, resulting in a 5 mm working distance. Two microprisms (one without coating and the other one coated with aluminum) are glued together and a miniature unfocused ultrasound transducer with 10 MHz central frequency and 2 mm aperture is mounted on the top of the cubic prism pair. The light beams are focused by the GRIN lens and reflected by the thin aluminum film to the tissue surface. The generated ultrasound waves transmit through the cubic prism group and are detected by the transducer. The backscattering photons from the tissue are reflected by the aluminum film and coupled into the same fiber through the GRIN lens. Figure 1(b) shows a photograph of the probe, where both the cubic prism pair and GRIN lens are 0.7 mm in diameter. A stainless steel tube 1.0 mm in diameter is used to protect the light path (i.e., the single-mode fiber, GRIN lens, and cubic prism pair). The probe is glued to the transducer and protected by another bigger stainless steel tube (2.3 mm in diameter).

The probe is mounted on a 3D linear stage (Fig. 2), and is scanned in 2D for 3D image formation. The light beam for ORPAM is generated from a pulsed Nd:YAG laser with 532 nm wavelength and a 10 Hz repetition rate. Two neutral density filters are used to attenuate the light energy, and a small iris is utilized to provide homogeneous light

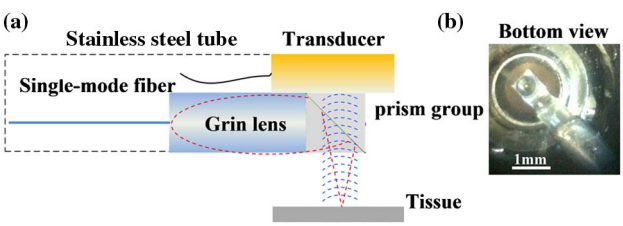

Fig. 1. (Color online) Schematic (a) and photograph (b) of the hybrid probe.

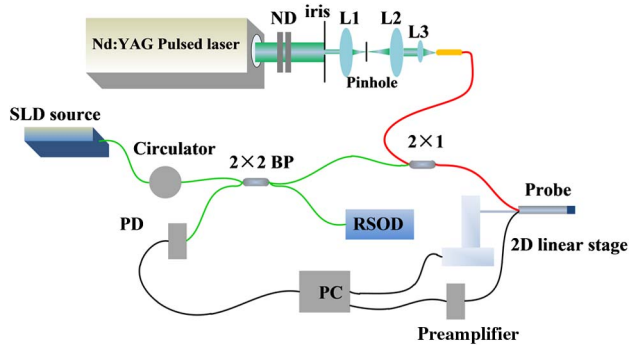

Fig. 2. (Color online) Schematic of the integrated ORPAM and OCT system. ND, neutral density; L1, lens 1; L2, lens 2; L3, lens 3; BP, beam splitter; PD, photodiode.

distribution. The shaped light beam is focused by a convex lens, which passes through a 50 μm pinhole for spatial filtering and is then coupled into a 2 × 1 beam coupler. The detected acoustic waves are amplified by two wideband amplifiers and digitized by a data acquisition (DAQ) board (NI5152, National Instrument) at a sampling rate of 250 MS/s.

A broadband light source (DenseLight, DL-BX9-CS3159A) with a center wavelength of 1310 nm is employed for OCT. The light source has a full width at half-maximum (FWHM) of 75 nm, providing an axial resolution of 10 μm in air. The broadband light is split into the reference arm and the sample arm by a beam splitter and coupled into the same 2 × 1 beam coupler used for ORPAM. The depth scanning from 0 to 1.6 mm at the reference arm is realized by a rapid scanning optical delay line (RSOD) coupled with a galvanometer scanning at 1 kHz. The OCT signal is then detected by a balanced photodetector, whose output is acquired and stored by a DAQ card. The sensitivity of the system is measured to be 74 dB.

The lateral resolution is determined by imaging a selected part of a USAF 1951 resolution test target. Figures 3(a) and 3(b) show the one-dimensional (1D) profile of three bars, where the smallest resolvable bar spacing is 15 μm (group 6, element 1). The three bars can be clearly identified by both OCT and ORPAM, indicating a lateral resolution of better than 15 μm. In tissue imaging, the scattering will reduce the spatial resolution of this probe; however, when the sample is optically thin, the degradation of lateral resolution is not significant [1]. The imaging depth of ORPAM is estimated to be 1.5 mm by imaging a pencil lead embedded in a turbid tissue mimicking phantom.

In our current probe, the size of the cubic prism pair (0.7 mm in diameter) is smaller than the aperture of the transducer (2 mm in diameter). Hence, the active area of the transducer is divided into two areas: one area indicated by A1 in Fig. 4(a) receives the photoacoustic signal transmitting through the cubic prism pair, and the other area (A2) collects the photoacoustic signal transmitting through water without going through the prism pair. Due to the different sound velocities in glass (3962 m/s) and

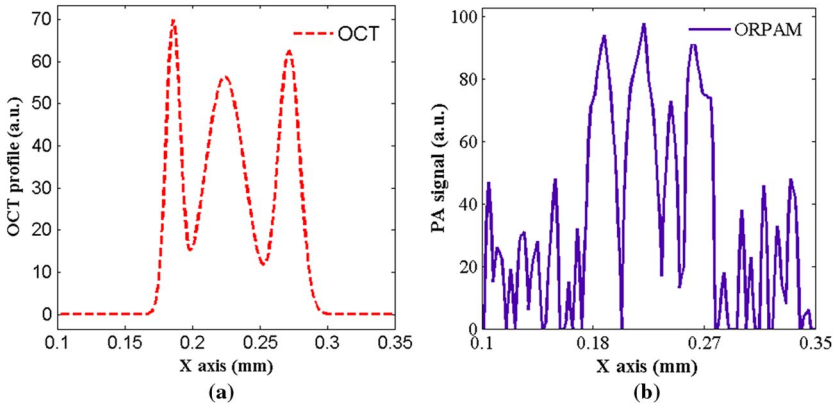

Fig. 3. (Color online) Resolution test for ORPAM and OCT. 1D profile of (a) OCT and (b) ORPAM of group 6, element 1.

water (1480 m/s), the photoacoustic signal received by A1 will arrive earlier than that received by A2 as indicated in Fig. 4(b). To compensate this difference, we calculated the time shift between the signals received by A1 and A2, and used the calculated time shift to calibrate the final signals for imaging. As shown in Fig. 4(c), the calibration allowed us to add the two signals together, resulting in improved signal-to-noise ratio (SNR) for image formation.

3. Results

To demonstrate the microscopic imaging ability of this dual-mode probe, we chose to image the ear of a mouse. Before starting the experiments, the hair on the ear was gently removed using a human-hair-removing lotion. The mouse was placed on a home-made animal holder and was anesthetized with a mixture of ketamine (85 mg/kg) and xylazine. After the experiments, the mice were sacrificed using University of Florida Institutional Animal Care and Use Committee (IACUC)-approved techniques. Strict animal-care procedures approved by the University of Florida IACUC and based on guidelines from the National Institutes of Health (NIH) for the Care and Use of Laboratory Animals were followed.

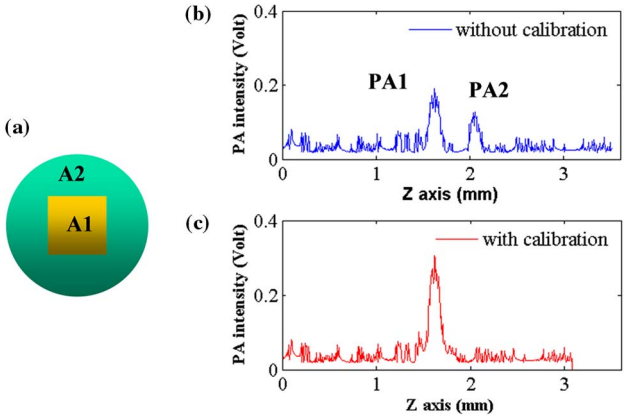

Fig. 4. (Color online) Signal calibration. (a) Schematic of the probe (bottom view). (b), (c) Typical A-line (Hilbert transform of raw data) without (b) and with (c) calibration.

The laser exposure was 25 mJ/cm^2 at the optical focus point, which is higher than the American National Standards Institute (ANSI) laser safety limit (20 mJ/cm^2) [14], but still below the reported skin-damage threshold [15]. The scanning step size was 6 μm along the X-Y plane.

The top rows of Figs. 5(a) and 5(b) show the maximum amplitude projection (MAP) images of ORPAM and OCT. OCT and ORPAM visualize different tissue structures: ORPAM clearly maps the microvasculature, while OCT images the sebaceous gland with high resolution. The bottom rows (cross section of tissue) of Figs. 5(a) and 5(b) show the benefits of combining these two modalities more clearly. The ear's thickness in the OCT image is from 400 to 600 μm. The dermal structure and the sebaceous gland are clearly observed. In the cross-sectional OCT, we can identify epidermis, dermis, and cartilage as indicated with yellow arrows. We have observed that ORPAM is good at locating microvessels in the ear with limited surrounding tissue information.

4. Discussion

The SNR of the ORPAM is 25 dB, which is lower than that of conventional ORPAM. There are several reasons contributing to the reduced SNR: (1) a 10 MHz ultrasound transducer was used in this probe, while it is known that the strongest generated acoustic signal lies between 30 and 70 MHz. (2) The transducer is flat, resulting in reduced sensitivity compared with a focused transducer commonly used in conventional ORPAM. (3) During the experiments, we used an 8 bit resolution DAQ card, which can only resolve signals larger than 40 mV. As a result, we lost some signals from small capillaries. These limitations, however, can be easily overcome using a miniature focused high-frequency transducer (>30 MHz), which will in turn improve the axial resolution of ORPAM and make the whole probe smaller as well. Using a high-resolution DAQ card will also help solve the aforementioned problems. (4) The actual resolution of a GRIN probe tends to be worse than this theoretical limit, because the effective NA of GRIN lenses is degraded, owing to the spatial aberrations in the lenses and misalignment between optical components.

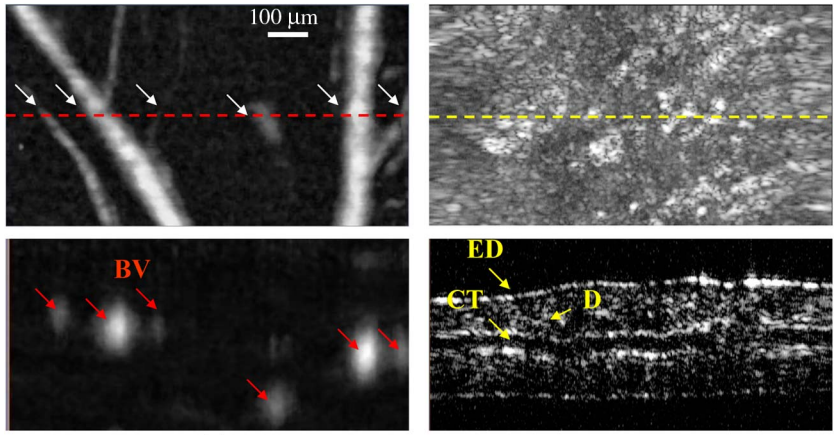

Fig. 5. (Color online) *In vivo* imaging of mouse ear by the integrated probe. MAP image (top) and cross section (bottom) of ORPAM (a) and OCT (b). ED, epidermis; CT, cartilage; D, dermis; BV, blood vessel.

For future improvements, we also need a suitable micromotor to implement an internal scanning mechanism and a faster laser to reduce the scanning time. Finally, we plan to replace the current slow time-domain (TD) OCT with fast frequency-domain (FD) OCT. These are necessary steps toward the clinical evaluation of ORPAM/OCT.

This work was sponsored in part by the J. Crayton Pruitt Family Endowment and by grants from the NSF and NIH.

References

1. K. Maslov, H. F. Zhang, S. Hu, and L. V. Wang, "Optical-resolution photoacoustic microscopy for in vivo imaging of single capillaries," Opt. Lett. **33**, 929–931 (2008).
2. S. Oladipupo, S. Hu, A. Santeford, J. Yao, J. R. Kovalski, R. Shohet, K. Maslov, L. V. Wang, and J. M. Arbeit, "Conditional HIF-1 induction produces multistage neovascularization with stage-specific sensitivity to VEGFR inhibitors and myeloid cell independence," Blood **117**, 4142–4153 (2011).
3. L. Xi, L. Zhou, and H. Jiang, "C-scan photoacoustic microscopy for in vivo imaging of Drosophila pupae," Appl. Phys. Lett. **101**, 013702 (2012).
4. L. Xiang, B. Wang, L. Ji, and H. Jiang, "4D photoacoustic tomography," Sci. Rep. **3**, 1113 2013 (online version).
5. L. Xi, S. R. Grobmyer, G. Zhou, W. Qian, L. Yang, and H. Jiang, "Molecular photoacoustic tomography of breast cancer using receptor targeted magnetic iron oxide nanoparticles as contrast agents," J. Biophotonics (2012).
6. L. Yin, Q. Wang, Q. Zhang, and H. Jiang, "Tomographic imaging of absolute optical absorption coefficient in turbid media using combined photoacoustic and diffusing light measurements," Opt. Lett. **32**, 2556–2558 (2007).
7. L. Xi, X. Li, L. Yao, S. Grobmyer, and H. Jiang, "Design and evaluation of a hybrid photoacoustic tomography and diffuse optical tomography (PAT/DOT) system for breast cancer detection," Med. Phys. **39**, 2584–2594 (2012).
8. Z. Yuan, Q. Zhang, and H. Jiang, "Simultaneous reconstruction of acoustic and optical properties of heterogeneous media by quantitative photoacoustic tomography," Opt. Express **14**, 6749–6754 (2006).
9. S. Jiao, M. Jiang, J. Hu, A. Fawzi, Q. Zhou, K. K. Shung, C. A. Puliafito, and H. F. Zhang, "Photoacoustic ophthalmoscopy for *in vivo* retinal imaging," Opt. Express **18**, 3967–3972 (2010).
10. E. Zhang, B. Povazay, J. Laufer, A. Alex, B. Hofer, B. Pedley, C. Glittenberg, B. Treeby, B. Cox, P. Beard, and W. Drexler, "Multimodal photoacoustic and optical coherence tomography scanner using an all optical detection scheme for 3D morphological skin imaging," Biomed. Opt. Express **2**, 2202–2215 (2011).
11. J. M. Yang, K. Maslov, H. C. Yang, Q. Zhou, K. K. Shung, and L. V. Wang, "Photoacoustic endoscopy," Opt. Lett. **34**, 1591–1593 (2009).
12. B. Wang, A. Karpiouk, D. Yeager, J. Amirian, S. Litovsky, R. Smalling, and S. Emelianov, "Intravascular photoacoustic imaging of lipid in atherosclerotic plaques in the presence of luminal blood," Opt. Lett. **37**, 1244–1246 (2012).
13. Y. Yang, X. Li, T. Wang, P. D. Kumavor, A. Aguirre, K. K. Shung, Q. Zhou, M. Sanders, M. Brewer, and Q. Zhu, "Integrated optical coherence tomography, ultrasound and photoacoustic imaging for ovarian tissue characterization," Biomed. Opt. Express **2**, 2551–2561 (2011).
14. Laser Institute of America, American National Standard for Safe Use of Lasers ANSI Z136.1-2007 (American National Standards Institute, 2007).
15. V. P. Zharov, E. I. Galanzha, E. V. Shashkov, N. G. Khlebtsov, and V. V. Tuchin, "*In vivo* photoacoustic flow cytometry for monitoring of circulating single cancer cells and contrast agents," Opt. Lett. **31**, 3623–3625 (2006).